Fast Echo Simulation and High Resolution Imaging of Distributed Targets under GEO SAR System

Yang Huang[1,a], Faguang Chang[1,b,*], Dexin Li[1,c], Zhen Dong[1,d] and Xing Chen[1,e]

[1]College of Electronic Science and Technology National University1 of Defense Technology (NUDT)Changsha 410073, China
a. huangyang18@nudt.edu.cn(Y.H.), b. cfg@nudt.edu.cn(F.C.), c. lidexin@nudt.edu.cn(D .L.)
d. dongzhen@nudt.edu.cn(Z.D.), e. chenxing13@nudt.edu.cn(X.C.)
**Faguang Chang*

Keywords: GEO SAR; distributed targets; echo simulation; improved SAR imaging algorithm; depth of focus.

Abstract: Since GEO SAR measured data are not available at present, all the echo simulation of GEO SAR is of great significance. However, the current research mainly focuses on the truth of the point target, and the research on the distributed targets is very few. Therefore, this paper focuses on the fast echo simulation of the distributed targets and the corresponding high resolution imaging technology under the GEO SAR system. Firstly, a geometric model of the surface object scene is established. Then an improved scene RD-ACS imaging algorithm is proposed for distributed targets scenes. Finally, the correctness of echo simulation and imaging is verified by experiments.

1. Introduction

Since the concept of GEO SAR was first proposed by K.Tomiyasu in 1978 [1], it has immediately attracted the attention of the whole SAR domain due to its ultra-long synthetic aperture time, very short re-entry period (about 24 hours), high resolution and quick response to emergencies. In the future, GEO SAR will play an important role in many fields such as seismic monitoring.

However, there are not many GEO SAR measured data available now, so the echo simulation work under the GEO SAR system is very meaningful. Now the simulation of GEO SAR echo is all about point or lattice target echo simulation. In the future practical application, distributed targets echo simulation is more meaningful, but there is little literature in this field. Moreover, in the GEO SAR system, due to the ultra- long synthetic aperture irradiation time and the asymmetric trajectory of the satellite, the space variation of range, azimuth and elevation will appear in the imaging processing, and there are few literatures on this aspect [2,3].Therefore, this paper focuses on the simulation of a fast distributed targets echo, and proposes an improved RD-ACS algorithm to achieve deep focus imaging of distributed targets.

The structure of this paper is as follows: Section II established the geometric model of the scene of the distributed targets. Section III introduces the proposed improved RD-ACS algorithm to solve the 3D space-variant problem. Section IV verifies the correctness of the simulation and imaging of the distributed targets echo through the simulation test. Section V summarizes this paper including a discussion on future research.

2. Geometric Modeling and Echo Simulation of Distributed Targets Scene

This part mainly analyzes the construction process of the distributed targets scene, through the combination relationship between the satellite and the target, the system of equations is established to solve the coordinate information of the target, and through interpolation processing to improve the calculation speed. Then the oblique distance between the target and the satellite is accurately obtained, and then the echo of each target in the scene is obtained. Finally, the echo of each target is coherently superplaced.

Since the satellite flight trajectory in GEO mode is nonlinear, it can be illustrated by the trajectory of sub-satellite points as shown in the figure.1. As shown in the figure below, trajectories of subsatellite points under different orbital inclinations are in the shape of "8", so the oblique distance history between the satellite and the target can no longer be obtained like that of classical SAR. Instead, the position and velocity vector of the satellite can be obtained according to the number of orbital roots of the satellite, and an accurate oblique distance model can be obtained.

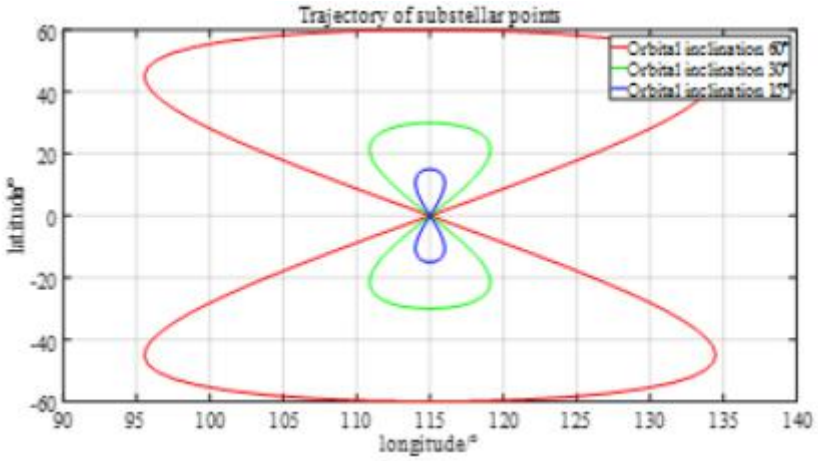

Figure 1: Trajectory of substellar points.

After the position of the satellite at different moments is obtained according to the six orbital roots, the direct point between the satellite at zero moment and the ground can be taken as the central point of the scene, and then the shortest distance between the satellite and the target can be taken as the independent variable to get each coordinate point on the scene of the plane target. The target of each point satisfies the following three conditions: the target is on the earth's ellipsoid, the shortest distance to the satellite is known, and the position vector of the target and the satellite is orthogonal to the velocity vector of the satellite at the time of the shortest distance, which can be referred to (1).Then get such a range- oriented element lattice at different azimuthal moments, and finally form the coordinates of the distributed targets position on the earth's surface.

$$\begin{cases} \dfrac{(x_t + y_t)^2}{r_e^2} + \dfrac{z_t^2}{r_p^2} = 1 \\ \left| P_{sat} - P_t \right| = R_n, n = 1, 2, \cdots, N_r \\ V_{sat}^{'} \cdot (P_{sat} - P_t) = 0 \end{cases} \tag{1}$$

where, x_t、y_t、z_t represents the target coordinates, r_e、r_p the earth equatorial radius and the polar radius of elliptical model, p_t and P_{sat} respectively represent the target position vector and the satellite position coordinate vector, R_n represents the different closest distances between the satellite and the target, N_r represents the number of points in the distance direction of the scene, V_{sat} is the velocity vector of the satellite, $(\cdot)'$ stands for transpose. The schematic diagram of the scene construction is shown below:

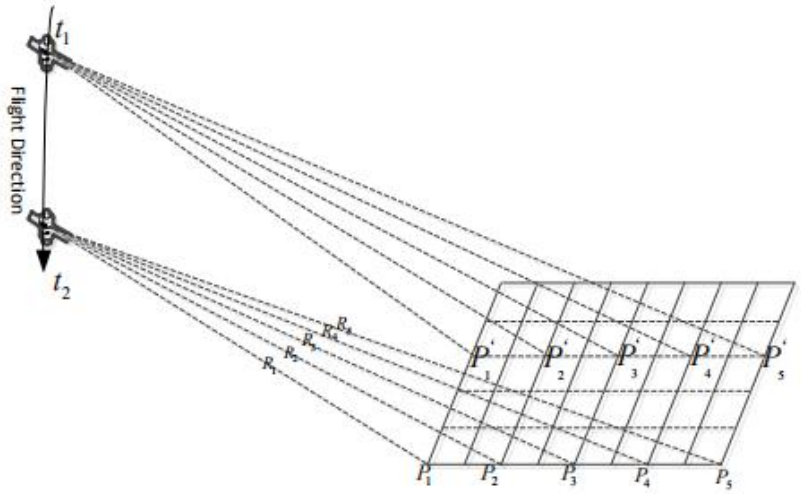

Figure 2: Scene construction diagram.

where, t_1 and t_2 denotes the satellite at two different azimuth moments, R_1、R_2、R_3、R_4 and R_5 represent the shortest distance of each range cell between satellite and the distributed targets P_1、P_2、P_3、P_4 and P_5 (or P_1'、P_2'、P_3'、P_4' and P_5') at the moment t (or t_2)

However, there will be a large number of scattering points in the scene of plane target, and it will produce a great amount of computation if the coordinates of scattering points are solved by solving the equations. Therefore, one of the innovations of this paper is to quickly obtain each scattering point target through interpolation only by figuring out several discrete and equally spaced points, as shown in (2) and (3) :

$$\begin{cases} R_n - R_{n-1} = \dfrac{c}{2f_s} \\ R_n' - R_{n-1}' = \dfrac{c \cdot \Delta n_r}{2f_s} \\ t_{a,n} - t_{a,n-1} = PRT \\ t_{a,n}' - t_{a,n-1}' = PRT \cdot \Delta n_a \end{cases} \tag{2}$$

$$\begin{cases} [XI, YI] = meshgrid(1 : \Delta n_r : N_r, 1 : \Delta n_a : N_a) \\ [xi, yi] = meshgrid(1:1:N_r, 1:1:N_a) \end{cases} \tag{3}$$

where, c is the speed of light, f_s is the sampling rate, $R_n' - R_{n-1}'$ is the difference of distance interval before interpolation, Δn_r is the number of distance cell interval, $t_{a,n} - t_{a,n-1}$ is the difference

of sampling time along the azimuth, Δn_a is the number of sampling time interval along the azimuth. The following figure 3 shows the coordinates calculated completely according to the solution equation and the scene coordinates obtained through interpolation:

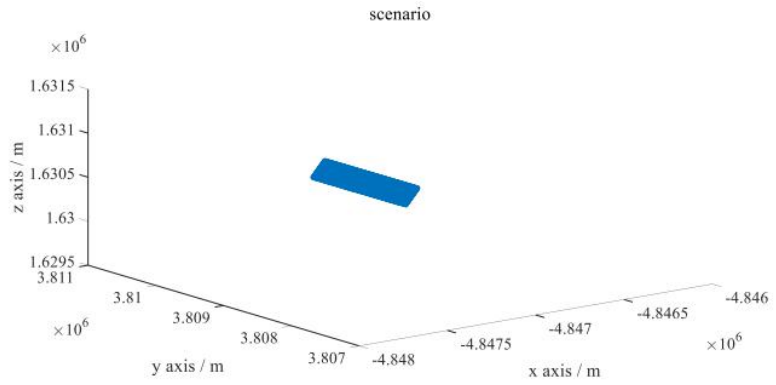

(a)The scene coordinates obtained according to the solution equation.

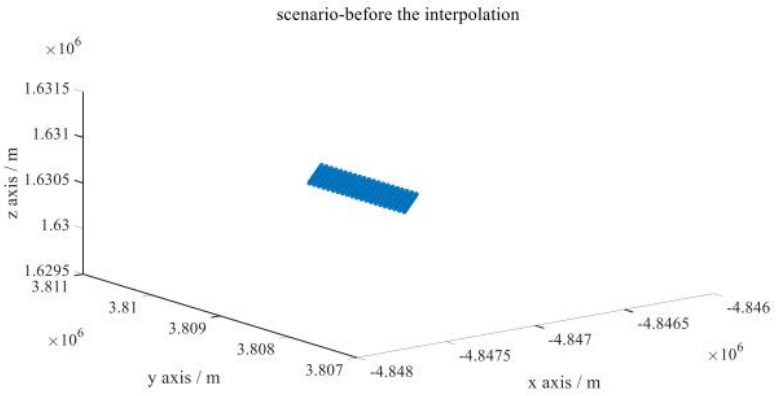

(b)Part scene coordinates are obtained according to the solution equation.

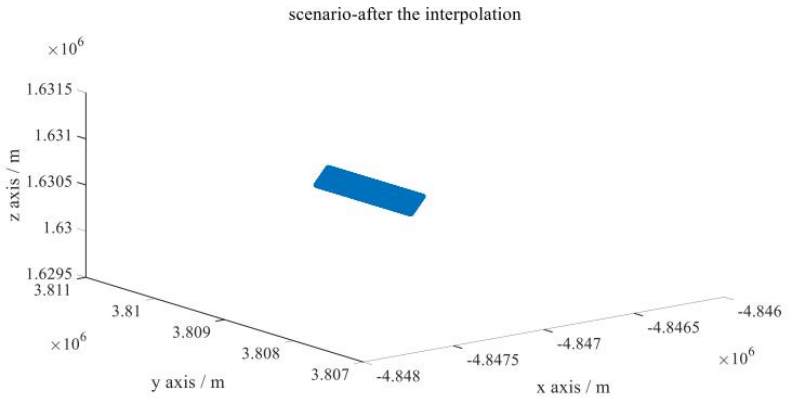

(c)The scene coordinates obtained after interpolation.

Figure 3: Scene coordinates.

According to (1) and (2), the scene coordinates on the surface plane can be solved, and the undulating terrain coordinates can also be obtained under the condition of known terrain elevation:

$$p_{t,h} = p_t \cdot \frac{|p_t| + h}{|p_t|} \tag{4}$$

where, and denotes the coordinate vector of the target and the elevation corresponding to the position, denotes taking the absolute value.After the trajectory changes of the satellite and the scene coordinates are obtained, the echoes of each scattered point in the scene can be accurately obtained:

$$\begin{cases} W_a = \left| \frac{\pi}{2} - \angle((P_{sat} - P_t), V_{sat}) \right| \le \frac{\theta_a}{2} \\ W_r = \left| t_r - \frac{2 \cdot r}{c} \right| \le \frac{T_r}{2} \\ phase = \pi \cdot k_r \cdot (t_r - \frac{2 \cdot R}{c})^2 - \frac{4 \cdot \pi \cdot R}{\lambda} \\ echo = e^{j \cdot phase} \cdot W_a \cdot W_r \end{cases} \tag{5}$$

where, W_a and W_r represents the limitation conditions in the azimuth and range directions, θ_a represents the width of the azimuth beam, t_r and T_r represents the fast time and pulse duration, represents the slant distance, k_r and λ represents the modulation frequency and wavelength, andrepresents the $phase$ and $echo$ data of each target. Finally, the echo of each point can be superimposed to get the scene echo.In this way, the default amplitude of each position is 1. In the Section IV, the scattering intensity of measured data will be used as input.

3. Improved RD-ACS Imaging Algorithm

In the GEO SAR system,due to the fundamental reason of asymmetric trajectory,the 3D space variation of range, azimuth and elevation has a serious impact on the focus depth.In this part, an improved algorithm is proposed to improve the focusing depth. In general, the first step in imaging processingis range compression, so the study is conducted directly from the echo signal after range compression:

$$\begin{aligned} s_{rc}(t_0, r_0; t_r, t_a; h_0) \approx A_0 w_r \left(t_r - \frac{2r(t_0, r_0; t_a; h_0)}{c} \right) \\ \cdot w_a(t_a - t_0) \cdot \exp\left(-j \frac{4\pi r(t_0, r_0; t_a; h_0)}{\lambda} \right) \end{aligned} \tag{6}$$

where, A_0 is the echo intensity as a constant, which can be ignored in the subsequent analysis, $w_r(\cdot)$ and $w_a(\cdot)$ is the envelope in the direction of range and azimuth respectively, $r(t_0, r_0; t_a; h_0)$ represents the sloping range history of the target. Since the height of the target is related to the position of the target, the elevation space variation can be decomposed into the 2D space variation of range and azimuth as well as their coupling. Through high-order Taylor expansion, the fifth order slant range model is generally accurate enough [4], so the high-order slant range model can be reconstructed as:

$$\begin{cases} r(t_0, r_0; t_a; h_0) = r_0 + \sum_{i=1}^{N} (k_i + \Delta k_i(t_0, r_0)) \cdot t_a^i \\ \Delta k_i(t_0, r_0) = \sum_{n=1}^{N} \left(\Delta k_{a,r} (r_0 - r_{0,c})^n + \Delta k_{a,a} (t_0 - t_{0,c})^n + \Delta k_{r,a} (r_0 - r_{0,c})(t_0 - t_{0,c}) \right) \end{cases} \tag{7}$$

where, $k_i, i = 1, 2, ..., N$ denotes the i-th coefficient of oblique distance, $\Delta k_i(t_0, r_0)$ denotes the coefficient of space variation $\Delta k_{a,r}$, $\Delta k_{a,a}$ and $\Delta k_{r,a}$ denotes distance, azimuth and coupling space

variation coefficient. Then, the center point of the scene is taken as the reference point, and through the principle of series inversion and stationary phase, (7) is substituted into (6) and transformed into the 2D frequency domain to perform bulk phase compensation [5,6].

After the bulk phase compensation, the range variation error compensation is carried out. Under the influence of range and elevation variation, the coefficient of high-order slant range model changes along with the range direction. In order to improve the focusing depth, this part of phase error must be compensated, which can be transformed into the range frequency domain azimuth-time domain. In terms of range migration and azimuth compression, $k_i, i=1,2,3,4,5$ is replaced by $k_{nr}(r)$, where the variable coefficient can be obtained for reference [7].

$$\begin{cases} \Delta R_{rcm}(r_0, f_a) \approx -\dfrac{c}{4\pi f_r}\left(\phi_{rcm}(r_0, \mathrm{f}_r, f_a) - \phi_{rcm}(\mathrm{f}_r, f_a)\right) \\ \Delta\phi_{ac}(r_0, f_a) \approx \phi_{ac}(r_{0r}, f_a) - \phi_{ac}(f_a) \end{cases} \tag{8}$$

where the subscript and represent range migration and azimuth compression. The residual range migration correction can be compensated by interpolation in the range-Doppler domain.

Since the azimuth compression phase changes with azimuth time and azimuth frequency, azimuth-time-varying compensation cannot be realized directly in the range-Doppler domain as the range space-varying compensation. Since onlyneed to consider the second and third order terms of the time varying coefficients and it's linear, the azimuth chirp scaling can be introduced to deal with the problem. The scaling function $A_a t_a^3 + B_a t_a^4$ can be introduced, and the slant distance model is:

$$\begin{aligned} r(t_a; t_0, r_0; h_0) \approx\ & r_0 + k_1(t_a - t_0) + \left(k_2 + \Delta k_{2,a}^{'} \cdot (t_0 - t_{0,c})\right)(t_a - t_0)^2 \\ & + \left(k_3 + \Delta k_{3,a}^{'} \cdot (t_0 - t_{0,c})\right)(t_a - t_0)^3 \\ & + k_4(t_a - t_0)^4 + k_5(t_a - t_0)^5 + A_a t_a^3 + B_a t_a^4 \end{aligned} \tag{9}$$

where, the solution of $k_{i,a}$ is the azimuth variation coefficient, and $t_{0,c}$ is usually zero. In the slant range model, in order to realize the time-invariance of the azimuth term, the coefficient of the linear term of t should be zero, and then the coefficient of the variable scale equation can be solved. After the time domain compensation of the azimuth time variation is completed, the data is changed to the range Doppler domain to compensate the errors introduced by the azimuth compression phase and the variable scale equation. The compensation phase can be obtained by using the principle of series inversion and stationary phase as follows:

$$\begin{cases} \varphi_{av,ac} \approx \dfrac{4\pi}{\lambda}\left(k_2 t_{a,s}^2(f_a) + (k_3 - A_a) t_{a,s}^3(f_a) + (k_4 - B_a) t_{a,s}^4(f_a) + k_5 t_{a,s}^5(f_a)\right) \\ \qquad + 2\pi f_a t_{a,s}(f_a) \\ t_{a,s}(f_a) \approx -\dfrac{\lambda f_a}{4k_2} - \dfrac{3(A_a + k_3)\lambda^2 f_a^2}{32k_2^3} - \dfrac{(9A_a^3 - 4B_a k_2 + 18A_a k_3 + 9k_3^2 - 4k_2 k_4)\lambda^3 f_a^3}{128k_2^5} \\ \qquad -5(((27A_a^3 - 24A_a B_a k_2 + 81A_a^2 k_3 - 24B_a k_2 k_3 + 81A_a k_3^2 + 27k_3^3 - \\ \qquad 24A_a k_2 k_4 - 24k_2 k_3 k_4 + 4k_2^2 k_5)\lambda^4) f_a^4) / (2048k_2^7) - 3(189A_a^4 - \\ \qquad 252A_a^2 B_a k_2 + 32B_a^2 k_2^2 + 756A_a^3 k_3 - 504A_a B_a k_2 k_3 + 1134A_a^2 k_3^2 - \\ \qquad 252B_a k_2 k_3^2 + 756A_a k_3^3 + 189k_3^4 - 252A_a^2 k_2 k_4 + 64B_a k_2^2 k_4 - 504A_a k_2 k_3 k_4 \\ \qquad -252k_2 k_3^2 k_4 + 32k_2^2 k_4^2 + 60A_a k_2^2 k_5 + 60k_2^2 k_3 k_5)\lambda^5 / (8192k_2^9) \end{cases} \tag{10}$$

The phase represents the azimuth compression phase of the azimuth variation, and represents the stationary phase point.When the range Doppler domain is multiplied by the frequency domain to compensate the phase, the azimuth time varying error can be compensated. Once the azimuth Fourier inverse changes, the focused result can be obtained. The following figure 4 is the research flow chart of the whole paper:

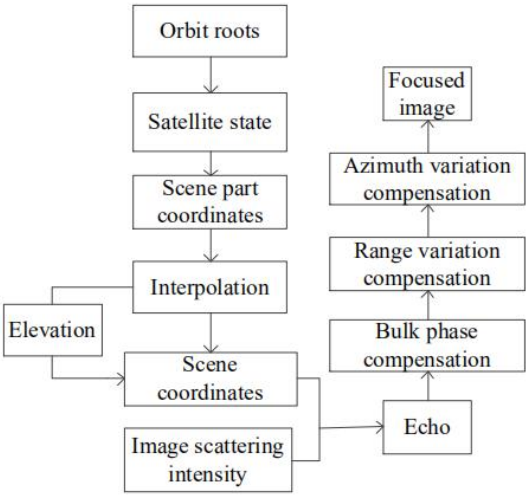

Figure 4: Paper processing process.

4. Experimental Verification

Table 1: System Paramenters.

Parameter	Value	Parameter	Value
Semi-major axis	42164.17Km	Right ascension of ascending	115°
Eccentricity	1×10^{-8}	Perigee	270°
Orbital inclination	60°	True anomaly	90°
Carrier frequency	9.514GHz	Antenna size	15 m × 15 m
Squint angle	0°	Incident angle	35.2°
Pulse duration	2.5 μs	Chirp bandwidth	30MHz

In order to verify the correctness of echo simulation, the measured data "Gaofen-3" imaging results were used as input to select some complex images with a size of 200*200, and the amplitude and phase of these points were brought into the echo simulation. System parameters are shown in Table 1.

The following figure 5 shows part of the complex images taken out, and then the classical CS algorithm and the improved RD-ACS algorithm are used for imaging respectively.

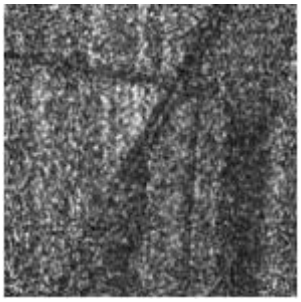
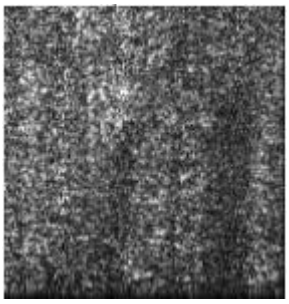
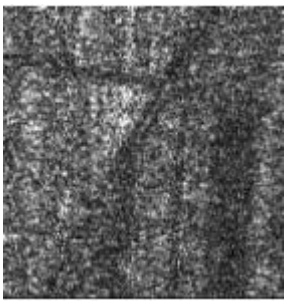

(a) Part of the image of "Gaofen-3" (b) CS algorithm (c) the improved RD-ACS algorithm

Figure 5: Imaging results.

The above is the plane scene directly obtained on the earth's surface, and the measured data is used as the input to obtain the imaging results. On the contrast, it can be seen that the improved RD-ACS algorithm can well restore the original terrain, while the classic CS algorithm is no longer applicable.In the following, the simulated cone is placed on the plane scene, and then the scattering intensity of the scene is obtained with the Georgia model to improve the imaging results obtained by the RD-ACS algorithm.

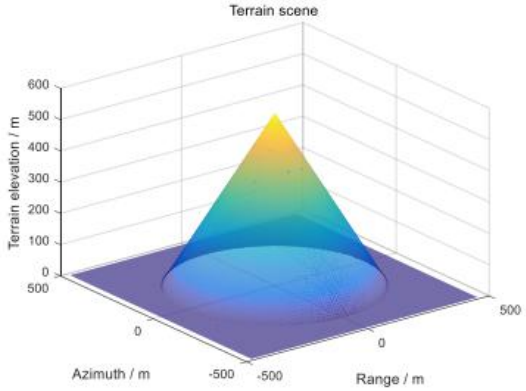

(a) Cone scenario.

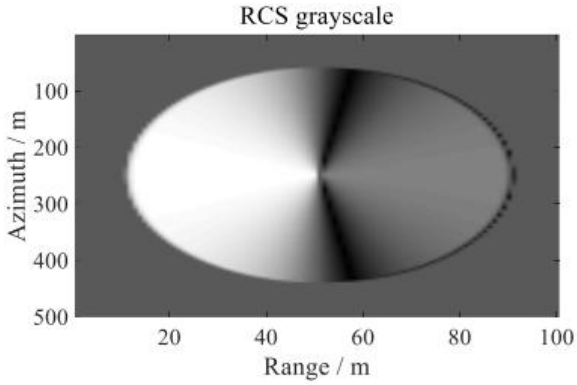

(b) Scene scattering intensity.

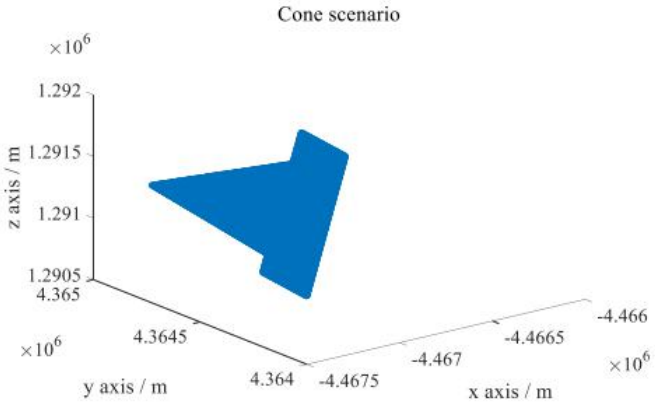

(c)Scene in the coordinate system.

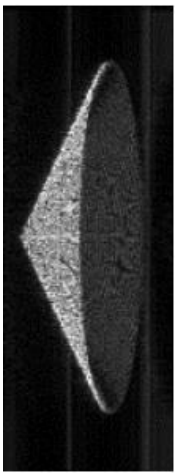

(d)Imaging result.

Figure 6: Cone scene and imaging results.

It can be seen that the RD-ACS algorithm can also achieve good focusing effect for cones with elevation information.

5. Conclusions

This paper mainly studies the echo simulation method of GEO SAR system, and proposes an improved RD-ACS algorithm according to the characteristics of GEO SAR. Due to the excessive synthetic aperture time of GEO SAR, a large amount of data will be generated. Therefore, in order to reduce the computational burden, the position coordinates of the scene can be quickly calculated by interpolation method, and the scene coordinates of undulating terrain can also be obtained according to the known elevation information of the terrain. In view of the space-variant problem that needs to be considered in GEO SAR, the 3D space-variant is decomposed into 2D space-variant by combining the relationship between terrain and position, and the space-variant error is compensated by range variation and azimuth variation. Finally, the correctness of echo simulation and imaging algorithm is verified by the measured data and simulation data respectively.In the future research, echo generation and high resolution imaging algorithm will be studied for more complex scenes.

Acknowledgments

The author is very grateful for anonymous reviewers for their valuable suggestions..

References

[1] Smith, K. Tomiyasu, "Synthetic aperture radar imaging from an inclined geosynchronous orbit," IEEE Transactions on Geoscience and Remote Sensing, vol. 21, pp. 324-328, 1983.

[2] Kou, L.; Xiang, M.; Wang, X.; Zhu, M. Tropospheric effects on L band geosynchronous circular SAR imaging. IET Radar Sonar Navig. 2013, 7, 693–701.

[3] Cheng Hu, Tao Zeng, et al. The accurate resolution analysis in Geosynchronous SAR[C]. European Conference on Synthetic Aperture Radar. 2010: 925-928.

[4] Cheng Hu, Tao Zeng, et al. The accurate resolution analysis in Geosynchronous SAR[C]. European Conference on Synthetic Aperture Radar. 2010: 925-928.

[5] Neo, Y.L., Wong, F.H., and Cumming, I.G.: 'A two-dimensional spectrum for bistatic SAR processing using series reversion', IEEE Geosci. Remote Sens. Lett., 2007, 4, (1), pp. 93–96.

[6] D. Li, M. Wu, Z. Sun, F. He, Z. Dong. Modeling and Processing of Two-Dimensional Spatial-Variant Geosynchronous SAR Data[J]. IEEE Journal of Selected Topics in Applied Earth Observations and Remote Sensing. Aug 2015, 8(8):3999–4009.

[7] Li, D.; Wu, M.; Sun, Z.; He, F.; Dong, Z. Modelling and Processing of Two-Dimensional Spatial-Variant Geosynchronous SAR Data. IEEE J. Sel. Topics Appl. Earth Observe. Remote Sens. 2015, 8, 3999–400.